Carbohydrate Polymers 114 (2014) 312–320

Contents lists available at ScienceDirect

Carbohydrate Polymers

journal homepage: www.elsevier.com/locate/carbpol

Bacterial cellulose/acrylic acid hydrogel synthesized via electron beam irradiation: Accelerated burn wound healing in an animal model

Najwa Mohamad [a], Mohd Cairul Iqbal Mohd Amin [a,*], Manisha Pandey [a], Naveed Ahmad [a], Nor Fadilah Rajab [b]

[a] Centre for Drug Delivery Research, Faculty of Pharmacy, Universiti Kebangsaan Malaysia, Jalan Raja Muda Abdul Aziz, Kuala Lumpur, Malaysia
[b] Biomedical Science Programme, Faculty of Health Sciences, Universiti Kebangsaan Malaysia, Jalan Raja Muda Abdul Aziz, Kuala Lumpur, Malaysia

ARTICLE INFO

Article history:
Received 22 May 2014
Received in revised form 20 July 2014
Accepted 5 August 2014
Available online 23 August 2014

Keywords:
Bacterial cellulose
Acrylic acid
Burn wound
Wound healing

ABSTRACT

Natural polymer-based hydrogels are of interest to health care professionals as wound dressings owing to their ability to absorb exudates and provide hydration for healing. The aims of this study were to develop and characterize bacterial cellulose/acrylic acid (BC/AA) hydrogels synthesized by electron beam irradiation and investigate its wound healing potential in an animal model. The BC/AA hydrogels were characterized by SEM, tensile strength, water absorptivity, and water vapor transmission rate (WVTR). The cytotoxicity of the hydrogels was investigated in L929 cells. Skin irritation and wound healing properties were evaluated in Sprague-Dawley rats. BC/AA hydrogels had a macroporous network structure, high swelling ratio (4000–6000% at 24 h), and high WVTR (2175–2280 g/m^2/day). The hydrogels were non-toxic in the cell viability assay. *In vivo* experiments indicated that hydrogels promoted faster wound-healing, enhanced epithelialization, and accelerated fibroblast proliferation compared to that in the control group. These results suggest that BC/AA hydrogels are promising materials for burn dressings.

1. Introduction

Health care personnel are faced with the difficulty of treating an increasing number of patients with wounds and burns (Mogoşanu & Grumezescu, 2014). Among the most complex types of burn to manage are partial- (second-degree) and full-thickness (third degree) burns, which require specialized dressings (Pham, Greenwood, Cleland, Woodruff, & Maddern, 2007). Numerous types of dressings are used to cover the wound surface in order to encourage healing. Hydrogel dressings have generated the greatest interest as dressings for burns because they produce an ideal hydration environment for healing (Yang, Zhu, Liu, Chen, & Ma, 2008). Hydrogels also have the ability to absorb exudates, and their transparency facilitates observation of the healing process (Boateng, Matthews, Stevens, & Eccleston, 2008). Additionally, hydrogels, three-dimensional polymers, have been widely investigated because of their biocompatibility with the human skin (Ito, Yoshida, & Murakami, 2013).

Natural product-based polymers are now widely used in regenerative medicine as dressings for wounds and burns, owing to their biocompatibility, biodegradability, and similarity to the extracellular matrix (Huang & Fu, 2010). Cross-linked natural polymers commonly used in hydrogel preparations include polysaccharides, homoglycans, chitin and chitosan, alginates, α-glucans, and β-glucans (Mogoşanu & Grumezescu, 2014). Recent studies have shown that bacterial cellulose (BC), synthesized by *Acetobacter xylinum* sp., has potential for use in wound dressings and artificial skin (Czaja, Krystynowicz, Bielecki, & Brown, 2006). BC and plant cellulose have similar chemical structures, the crystallinity, mechanical strength, and absorption capacity of BC are greater than those of plant cellulose, which has led to the utilization of BC in the biomedical field (Shah, Ul-Islam, Khattak, & Park, 2013). Due to its various unique properties, BC has been recommended as an alternative dressing for partial-thickness burns (Fu, Zhang, & Yang, 2013).

Natural product-based polymers are commonly cross-linked with synthetic polymers to ensure that the hydrogel can entrap water and prevent dissolution of the hydrophilic polymer chains in an aqueous environment. Numerous crosslinking methods have been developed for the production of hydrogels. Current techniques include chemical crosslinking, polymerization with crosslinking agents, and high-energy radiation-induced crosslinking. The

* Corresponding author. Tel.: +60 3 9289 7690; fax: +60 3 2698 3271.
E-mail addresses: mciamin@pharmacy.ukm.my, mciamin@yahoo.co.uk (M.C.I. Mohd Amin).

http://dx.doi.org/10.1016/j.carbpol.2014.08.025
0144-8617/

irradiation-induced cross-linking technique provides sterilization and hydrogel crosslinking in a single step. The physical properties of hydrogels produced in this manner are dependent on the degree of crosslinking and polymer composition (Soler, Rodríguez, Correa, Moreno, & Carrizales, 2012). This method also provides an alternative to the use of chemical initiators and crosslinkers, which can be harmful and difficult to remove (Yang et al., 2008). Poly(vinyl alcohol), poly(ethylene glycol), and poly(acrylic acid) are common synthetic polymers that are cross-linked to form hydrogels by using a high-energy irradiation process.

In our previous study, BC was combined with AA (acrylic acid) at several ratios was used to fabricate hydrogels by exposure to accelerated electron beam (EB) irradiation at different doses. The Fourier transform infrared spectroscopy (FTIR) results revealed that AA had been successfully grafted onto the cellulose fibers. Morphological analysis showed that hydrogels prepared by the mixture of BC and AA had a highly macroporous sponge-like structure. Pore size in the hydrogels decreased as AA content and irradiation doses increased (Amin, Ahmad, Halib, & Ahmad, 2012). These hydrogels exhibited many promising features for an effective wound dressing.

The highly macroporous structure and water absorption capability of bacterial cellulose acrylic acid (BC/AA) hydrogels may be beneficial for exudate absorption and preservation of moisture in the wound area. Furthermore, the degree of crosslinking of these hydrogels can be fine-tuned by varying the irradiation dose. This can be helpful to controlling the mechanical strength and water absorption capacity of the hydrogels.

The objectives of this study were to develop and characterize BC/AA hydrogels synthesized by EB irradiation specifically used for wound dressing material and investigate its wound healing potential in an animal model. We studied in particular the physical and mechanical properties, and cytotoxicity of hydrogels fabricated by EB irradiation at doses of 35 kGy (H_{35}) or 50 kGy (H_{50}). Furthermore, the effects of H_{35} on normal skin and on healing of partial-thickness burns were evaluated in rats.

2. Experimental

2.1. Materials

BC was prepared from *nata de coco* (coconut water fermented by *A. xylinum*) that had been purified as reported earlier (Amin, Abadi, & Katas, 2014). AA and phosphate-buffered saline (PBS) were supplied by Sigma–Aldrich (USA). Distilled water was used to prepare aqueous solutions and dispersions. Petri dishes (90 mm × 13 mm) were used as molds for the preparation of hydrogels. Isoflurane was supplied by Piramal Healthcare (India).

2.2. Preparation of BC/AA hydrogels

The BC/AA hydrogel was prepared as described by Amin et al. (2012). Purified BC was ground to a powder (particle size 20–200 μm). AA was added to a 1% (w/v) dispersion of BC in distilled water to produce a 40:60 AA:BC mixture, which was mixed using a mechanical homogenizer (IKA Labortechink Ultra Turrax T25, Germany) at room temperature (26 °C) for 30 min to ensure thorough mixing. This mixture was poured into petri dishes (10 mL/dish) for exposure to electron-beam radiation at 35 and 50 kGy in air at the accelerator facility (NHV-Nissin High Voltage, EPS 3000, Japan) at the Malaysian Nuclear Agency.

2.3. Gel fractions of hydrogels

Freshly prepared hydrogels were cut into disks (1 cm diameter, 0.7–1.0 mm thick) and dried in an oven at 60 °C to a constant weight. The dried hydrogels were then subjected to extraction in distilled water with the distilled water replaced twice a day for 2 weeks. This ensured removal of un-reacted monomers so that only purified hydrogel would be subjected to analysis. The extracted hydrogels were dried in an oven at 60 °C to a constant weight. The gel fraction (%) was calculated using the following Eq. (1):

$$G_F(\%) = \frac{G_d}{G_i} \times 100 \quad (1)$$

where G_d is the initial dried weight before extraction and G_i is the constant dried weight of the hydrogels after extraction.

2.4. Film thickness

The film thickness of dried extracted hydrogels was measured using a micrometer (Digimatic Micrometer MDC-S, Mitutoyo Co., Japan) with 0.001 mm accuracy (Rhim, 2004). Five measurements were taken for each sample.

2.5. Water absorptivity study

The degree of swelling of the hydrogels was performed according to a previously described method (Wang, Zhu, Xue, & Wu, 2012). Dried and weighed hydrogels disks were immersed in 50 mL PBS (pH 7.4, 37 °C) and the swollen samples were weighed at specific intervals. The degree of swelling (2) and moisture content (3) in PBS were calculated using the following equations:

$$\text{Swelling ratio}(\%) = \left[\frac{H_s - H_d}{H_d}\right] \times 100 \quad (2)$$

$$\text{Moisture content ratio}\,(\%) = \left[\frac{H_s - H_d}{H_s}\right] \times 100 \quad (3)$$

where H_s and H_d are the weights of swollen and dried hydrogels. The experiments were performed in triplicate and the average of the results was reported.

2.6. Water retention properties

Moisture conservation in the hydrogels was evaluated by a water retention test (Lin, Lien, Yeh, Yu, & Hsu, 2013). After measuring the initial dry weights (M_{dry}), the hydrogels were immersed in PBS for 24 h. The swollen hydrogels were then wiped with filter paper to remove surface water and placed in petri dishes at room temperature. The samples were weighed (M_{wet}) after specific periods. The moisture retention ratio was calculated using the following Eq. (4):

$$\text{Moisture retention ratio}\,(\%) = \frac{M_{wet} - M_{dry}}{M_{dry}} \times 100 \quad (4)$$

2.7. Water vapor transmission

The water vapor transmission (WVT) of the hydrogel was measured using previously described methods (Lin et al., 2013). Briefly, hydrogels (diameter 1.1 cm) were mounted on the brim individual glass vials containing 20 mL of distilled water. The hydrogels were fastened to the vials with rubber rings, and the vials were placed in a humidity chamber (Terchy HRM 80 FA, Taiwan) at 37 °C and 84% humidity. The evaporation of water through the hydrogel was determined by weighing the vials once per hour for 8 h, and then at 24 and 48 h. A weight decrease was taken to indicate the loss of water. The profile of weight loss was plotted versus time for each sample. The water vapor transmission rate (WVTR) was calculated by dividing the daily weight loss of water by the area of the vial opening.

2.8. Mechanical properties

Tensile strength and percentage elongation at the breaking point of the hydrogels were evaluated using a Universal Testing Machine (Texturometer TA XT2i, Stable Microsystems, UK). These mechanical properties were tested by stretching dumbbell-shaped specimens (30 mm × 4 mm) to their breaking points at a crosshead speed of 5 mm/min. Force and elongation were measured when the hydrogel films broke. The tensile strength (5) and percentage elongation at break (6) were calculated as follows (Khan, Peh, & Ch'ng, 2000):

$$\text{Tensile strength}\,(\text{N/mm}^2) = \frac{N_{\text{break}}}{A_{\text{sample}}} \quad (5)$$

$$\text{Elongation at break}\,(\%) = \frac{L_{\text{break}}}{L_{\text{original}}} \times 100 \quad (6)$$

where N_{break} is the maximum load (N) required to break the film, A_{sample} is the cross-sectional area of the sample (mm^2), L_{break} is the increase in length at the breaking point (mm), and L_{original} is the original length of the film (mm).

2.9. Scanning electron microscopy (SEM)

Surface morphologies of the hydrogel samples were studied by SEM (LEO 1450 VPSEM, Zeiss, Germany) using a tungsten filament. Specimens were mounted on an aluminum stub with double-sided carbon tape and coated with gold in a sputter coater (SC500, Biorad, UK) in an argon atmosphere. The coated hydrogel were observed under SEM at 30× magnification and 15 kV.

2.10. In vitro cytotoxicity studies

2.10.1. Cell viability study

The L929 (mouse fibroblast) cell line (American Type Culture Collection, ATCC, USA) was used for the cell viability experiments. Cells were cultured in advanced minimal essential medium (MEM) with 110 mg/L sodium pyruvate and non-essential amino acids and without L-glutamine (Gibco™, Life Technologies, USA), supplemented with 10% fetal bovine serum (Sigma–Aldrich, USA) and 1% penicillin/streptomycin (Thermo-Fisher Scientific, USA) at 37 °C under 5% CO_2. The culture medium was refreshed every 2 days.

Changes in cell viability produced by the hydrogels were evaluated by indirect and direct cytotoxicity tests using alamarBlue® (Invitrogen, USA), (O'Brien, Wilson, Orton, & Pognan, 2000). The cytotoxic effects of hydrogels produced using different doses of radiation were evaluated. The indirect method was carried out by seeding L929 cells into 96-well plates (1×10^4 cells/well) followed by incubation overnight. The hydrogel extract was prepared by incubating sterilized 1.5 cm diameter hydrogel disks with 1 mL culture medium at 37 °C overnight. After incubation, 100 μL of the media extract was transferred into each well (Kumar et al., 2010). For direct cytotoxicity tests, 1.5 cm diameter hydrogel disks were incubated with 1 mL of culture medium in 24-well plates for 24 h and L929 cells were seeded onto these hydrogels (5×10^4 cells/well) (Yu et al., 2013).

Cells from the indirect and direct tests were incubated for 24 and 48 h and tested with the alamarBlue® assay. The optical densities were measured at 570 nm with a 600 nm reference wavelength using a microplate spectrophotometer (Infinite® M200 Pro Nanoquant Tecan, Switzerland). The percentage of viable cells was calculated using the following formula (7):

$$\%\,\text{cell viability} = \frac{A_{\text{hydrogel}}}{A_{\text{control}}} \times 100 \quad (7)$$

where A_{hydrogel} is the absorbance at 570 nm of the cells with hydrogel, and A_{control} is the absorbance at 570 nm of the control cells.

2.10.2. Cell attachment studies

The growth of L929 cells on the hydrogels was qualitatively analyzed using SEM as previously reported (Han, Tu, Zeng, Zhao, & Zhou, 2012) with some modifications. L929 cells were seeded onto hydrogels in 24-well plates (5×10^4 cells/well). After 3 days, the hydrogels were washed with PBS for 30 min and fixed with 4% formaldehyde in PBS for 30 min at 4 °C. Then the hydrogels were dehydrated with serial dilutions of alcohol, then prepared for SEM and observed as described above.

2.11. Animal studies

The wound healing characteristics of the H_{35} hydrogel preparation was evaluated in a rat model. All experiments were performed with the approval of the Universiti Kebangsaan Malaysia Animal Ethics Committee (UKMAEC). Female Sprague-Dawley rats ($N = 62$) weighing 150–200 g were obtained from the laboratory animal resource unit of Universiti Kebangsaan Malaysia (UKM). The rats had access to a standard diet and water *ad libitum*. The rats were maintained in a controlled environment with a 12-h light/12-h dark cycle at 24 °C ± 2 °C and 60 ± 5% humidity.

2.11.1. Dermal irritation tests

Dermal irritation tests were performed using Sprague-Dawley rats ($n = 4$ per group). A 5 cm × 5 cm dorsal area was shaved with an electric razor. After 24 h, the H_{35} hydrogels were placed on the backs of the rats in the experimental group, while Intrasite Conformable® hydrogels were used for the positive control group. Samples were taken at 1 h, 4 h, 24 h, and 48 h to evaluate skin reactions such as erythema and edema (Han et al., 2012).

2.11.2. Establishment of skin burns

The rats were anesthetized by isoflurane inhalation. The dorsal area of each rat was shaved and disinfected with 70% alcohol. Partial-thickness burns were produced on the shaved area by a 10 s application of a 1 cm diameter stainless steel template that was heated in boiling water for 5 min (Loo et al., 2014).

2.11.3. Treatment of burns wounds

The rats were divided into three groups ($n = 6$/group). Treatments were applied to each burn shortly after it was produced and rinsed with 70% alcohol. Group 1 animals were treated with H_{35}, group 2 was treated with Intrasite Conformable® hydrogel (positive control), and group 3 received no treatment (negative control). The treatments were applied to the wounds daily for 14 days after cleaning with alcohol (Loo et al., 2014). After positioning the dressings, bandaging tape (3 M™ Vetrap™, USA) and surgical tape (TOP-UKO, Malaysia) were used to secure them, and wounds were allowed to heal. All rats were housed in individual cages.

2.11.4. Visual observation of wound closure

Standardized digital photographs of the wounds were taken after 1, 3, 7, and 14 days during replacement of the dressings. Each photograph was taken at the same position with a ruler placed at the bottom (proximal end) of the wound. The burn wound size for each animal was measured at specific times to calculate the percentage of wound closure (8) using the following equation (Alsarra, 2009):

$$\%\,\text{wound closure} = \left[\frac{A_0 - A_t}{A_0}\right] \times 100 \quad (8)$$

where A_0 is the original burn wound area and A_t is the burn wound area at the time of observation.

Table 1
Thickness, gel fraction, tensile strength, and elongation at breaking of H_{35} and H_{50} hydrogels (data expressed as mean ± SD).

Hydrogel (kGy)	Thickness (mm)	Gel fraction (%)	Tensile strength (N/mm^2)	Elongation (%)
35	0.78 ± 0.05	73.70 ± 0.20	1.39 ± 0.21	377.74 ± 23.2
50	1.19 ± 0.03	85.75 ± 0.14	0.95 ± 0.16	164.45 ± 6.51

2.12. Histological analysis

Animals were euthanized on days 1, 7, and 14. Excised burn sites were fixed with formaldehyde (10%), and embedded in paraffin. The samples were cut into sections (4 μm) with a cryomicrotome (Leica RM 2145, Germany). After tissue sections were dewaxed and rehydrated, sections were stained with hematoxylin and eosin (H&E) and Masson's trichrome stain. The stained samples were examined using an optical microscope (Olympus, BX41TF, Japan) under 20× and 40× magnification.

2.13. Statistical analysis

Statistical analysis was carried out using (IBM SPSS software version 21, USA). Differences between means were analyzed for statistical significance using Student's *t*-test and One Way ANOVA. All data are presented as mean ± standard deviation (SD).

3. Results and discussion

3.1. Characterization of hydrogel

3.1.1. Film thickness and gel fraction

The thickness of the hydrogel and the gel fraction changed significantly depending on the hydrogel preparation, as shown in Table 1. The H_{50} hydrogel sheet (1.19 mm) was significantly thicker than the H_{35} sheet (0.78 mm). The gel fraction of the H_{50} hydrogel was significantly greater than that of the H_{35} hydrogel. Therefore, the gel fraction increased as the radiation dose increased. The thickness and gel fraction of the hydrogels was increased at higher electron-beam irradiation dose because of increased crosslinking of AA monomers and BC at higher irradiation dose (Halib, Amin, & Ahmad, 2010).

3.1.2. Water absorptivity and water retention

The swelling and water content of the hydrogels are shown in Fig. 1a and b. The swelling ratios of H_{35} and H_{50} at 24 h were approximately 6000% and 4000%, respectively, and the corresponding water content ratios were approximately 98% and 97%. The swelling percentage decreased as the irradiation dose increased, perhaps because of an increase in the degree of crosslinking (Ajji, Mirjalili, Alkhatab, & Dada, 2008). Hydrogel swelling is an important feature of dressings. Large water absorption capacities allow hydrogel dressings to absorb wound fluids and exudates (Yang et al., 2008). As shown in Fig. 1c, the water retention ratios for H_{35} and H_{50} hydrogel preparations were approximately 30% and 18% after 48 h, respectively. H_{35} hydrogel retained significantly more water after 48 h than H_{50} hydrogel because of its highly porous structure, which resulted in greater initial water penetration (Halib et al., 2010). Based on the swelling and water retention ratios of the H_{35} and H_{50} hydrogel preparations, H_{35} hydrogel may more effectively maintain a moist environment and prevent scab formation and dehydration of the wound bed.

3.1.3. WVTR

An ideal wound dressing should maintain an optimal rate of evaporative water loss. WVTRs for the hydrogels are shown in Fig. 1b. The WVTR for H_{35} and H_{50} hydrogels were approximately 2175 and 2280 g/m^2/day, respectively, which are within the acceptable range to maintain an optimal environment for wound healing (Lee, Chang, Yang, Chien, & Lai, 2012). This property may be associated with the COOH group in AA and the non-substituted hydroxyl group of cellulose, which efficiently retained water molecules through strong hydrogen bonding (Halib et al., 2010).

The moisture permeability of the hydrogels prevents fluid accumulation in an exudating wound. An important feature of hydrogel dressings is the control of absorption and transmission of wound exudates, and the ability to accelerate cell migration and

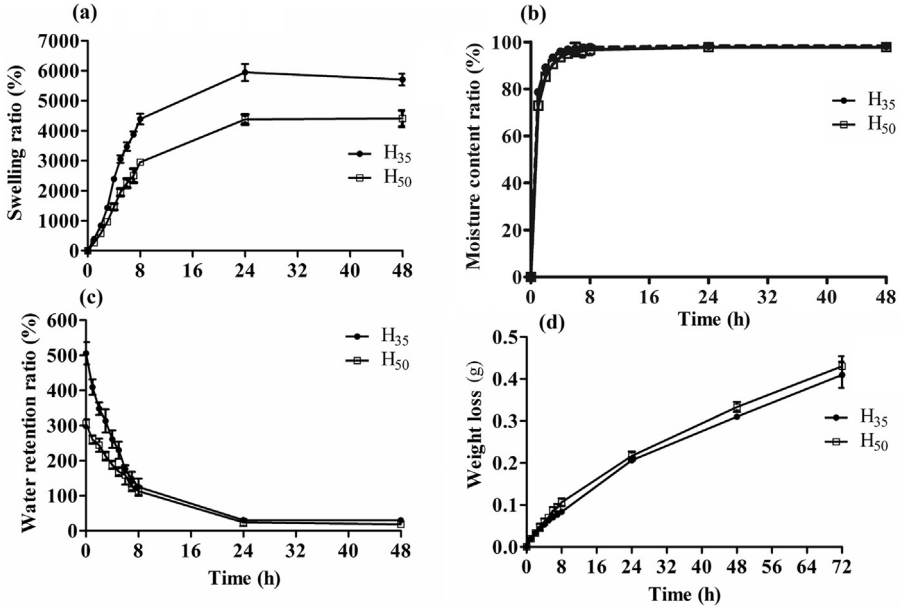

Fig. 1. Physical characteristics of H_{35} and H_{50} hydrogels: (a) swelling ratio, (b) moisture content ratio, (c) water retention ratio, and (d) water vapor transmission rate profile.

epithelialization in the wound area by maintaining high humidity. Low WVTRs can cause exudate accumulation, which may inhibit healing and increase the risk of infection (Kim et al., 2007).

3.1.4. Mechanical properties

The tensile strength and elongation tests provided an evaluation of the strength and elasticity of the hydrogel films. The mechanical properties of the films were evaluated as shown in Table 1. H_{35} films showed significantly greater elongation (377%, $p < 0.05$) before breaking and required significantly more force to break ($1.39\ N\ mm^{-2}$) compared to H_{50} films.

Higher radiation energy produced greater numbers of radical species, which created active sites on AA that facilitated the grafting process and increased crosslinking (Said, Alla, & El-Naggar, 2004). Increasing crosslinking resulted in a stronger, but more brittle, hydrogel. Thus, there is an optimal degree of crosslinking that produces a relatively strong, yet elastic, hydrogel (Peppas, Bures, Leobandung, & Ichikawa, 2000).

In the present study, H_{35} hydrogel exhibited higher tensile strength than H_{50}. A higher degree of crosslinking creates a thicker, more brittle and less elastic hydrogel, which requires less force to break. The greater elasticity and tensile strength of the H_{35} preparation should produce a soft, elastic hydrogel film that follows skin movements and possesses adequate resistance to mechanical abrasion (Boateng et al., 2008).

3.1.5. SEM studies

The SEM images of the hydrogel sheets produced with different radiation doses are shown in Fig. 2. At 30× magnification, the macroporous surface structure of the H_{35} preparation was apparent, with pore sizes ranging from 23.61 to 82.38 μm, while the H_{50} preparation had pore sizes from 34.62 to 61.44 μm. The superporous surface structure showed pores in the H_{35} preparation from 120.90 to 876.50 μm, while pores in the H_{50} preparation showed a reduced size (118.00–497.20 μm). Porous hydrogels are divided into macroporous (1–100 μm pores) and superporous (10–1000 μm pores) hydrogels depending on the pore size (Kim & Park, 2004). In these preparations, higher EB radiation dose increased the degree of crosslinking between AA and BC and formed a denser network structure and decreased pore size. The porous structure of H_{35} formed an interconnected network of channels that allows water molecules to diffuse in every direction (Halib et al., 2010). An increase in hydrogel pore density allows a dressing to more effectively absorb wound fluids and keep the wound dry. Despite increased fluid uptake, the interconnected pores of hydrogel dressings permit the transport of nutrients to cells, which promotes migration, proliferation, and differentiation (Zaborowska et al., 2010).

3.2. Cell viability and cell attachment

A primary requirement for any biomedical material is that it must be biocompatible, which is the ability of the material to perform with an appropriate host response in a specific situation (Williams, 1999). The biocompatibility of H_{35} and H_{50} was examined by measuring cytotoxicity after indirect and direct contact. Cytotoxicity results for H_{35} and H_{50} hydrogel sheets on L929 cells are shown in Fig. 3a (indirect) and 3b (direct). After 24 h incubation with extracts of H_{35} and H_{50}, cell viability was 98.26% and 98.14%. During the same period, cell viability after direct contact with H_{35} and H_{50} was found to be 94.50% and 91.88%. Cell viability after 48 h incubation with extracts of H_{35} and H_{50} was 89.71% and 87.41% while after direct contact, cell viability was 86.83% and 85.15%. By both methods, the viability of the cells incubated with H_{50} was lower ($p < 0.05$) than cells incubated with H_{35}. This could be due to the presence of a higher number of COOH groups in the AA of the H_{50} sheets, which may have led to a more acidic environment, as previously reported (Gupta, Plummer, Bisson, Frey, & Hilborn, 2002). Comparison between direct and indirect methods showed no significant difference in terms of cell viability ($p > 0.05$). The percentage of viable cells after indirect and direct contact at 24 h and 48 h were more than 85% for both hydrogels. It has been suggested that any wound dressing that results in cell viability greater than 85% can be considered non-toxic for use as a wound dressing (Lin et al., 2013). Thus, H_{35} and H_{50} hydrogel preparations would be considered safe based on their effects on L929 cells.

The attachment of L929 cells to the hydrogel was analyzed using SEM. Fig. 3c and d show attached cells on the surface of the H_{35} and H_{50} hydrogels. The images showed that the cells maintained an oval morphology on the hydrogels. These results demonstrated that the hydrogels are biocompatible and may be safe for use as wound dressings.

3.3. Animal studies

The physical characterization of the hydrogels indicated that H_{35} showed greater water absorption capacity, water retention, elasticity, and mechanical strength than H_{50}. Thus, H_{35} was investigated for its potential as a wound dressing to heal burns in rats.

3.3.1. Dermal irritation tests

Dermal irritation reactions were observed at 1 h, 4 h, 24 h, and 48 h. No erythema or edema was observed on the skin. The H_{35} hydrogel did not induce any skin irritation and appears to be a biocompatible material that can be used for dressing burns.

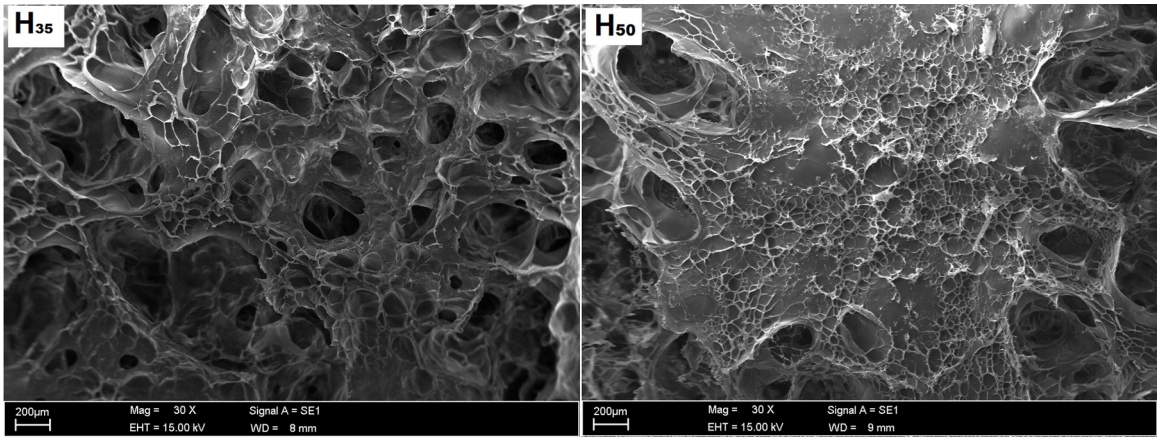

Fig. 2. SEM images of the H_{35} (0.78 mm) membrane and H_{50} (1.19 mm) membrane at 30× magnification.

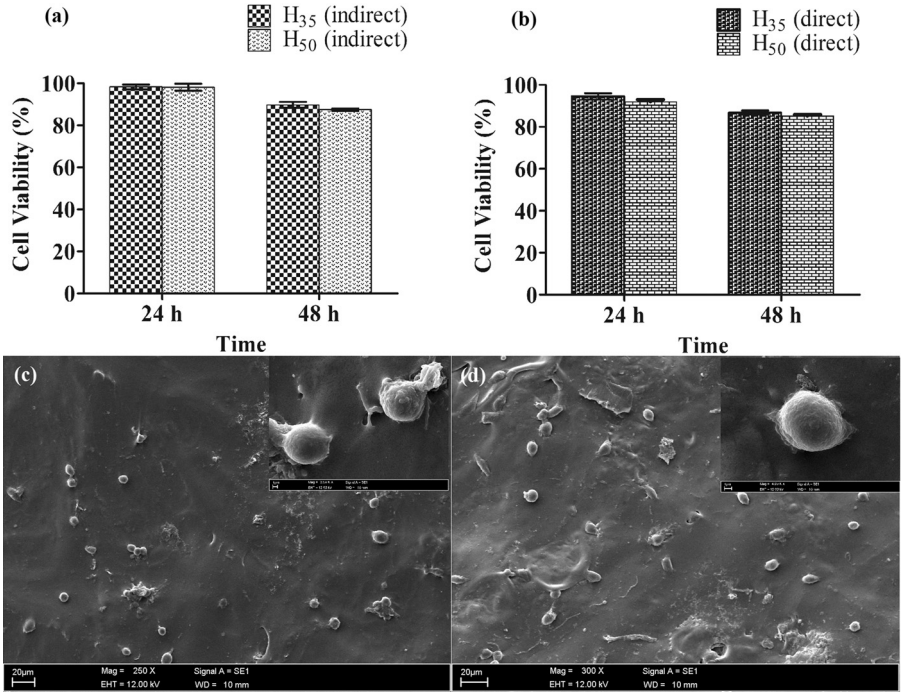

Fig. 3. Cytotoxicity of H_{35} and H_{50} on mouse fibroblast L929 cells: (a) indirect method (24 h and 48 h incubation), (b) direct method (24 h and 48 h incubation), (c) cell attachment on H_{35}, and (d) cell attachment on H_{50}.

3.3.2. *Wound closure*

Macroscopic observations of wound closure, as shown in Fig. 4, revealed clear differences between the H_{35}-treated and control groups. Each burn was observed for at 1, 3, 7, and 14 days post-injury. At days 1 and 3, inflammation (redness and swelling) was observed at the burn site. This suggested that the inflammatory phase began within a few minutes to 24 h after the injury and lasted for approximately 3 days (Boateng et al., 2008). No signs of infection or a reduction in burn size were observed at these initial time points. At day 7 post-injury, the untreated control group

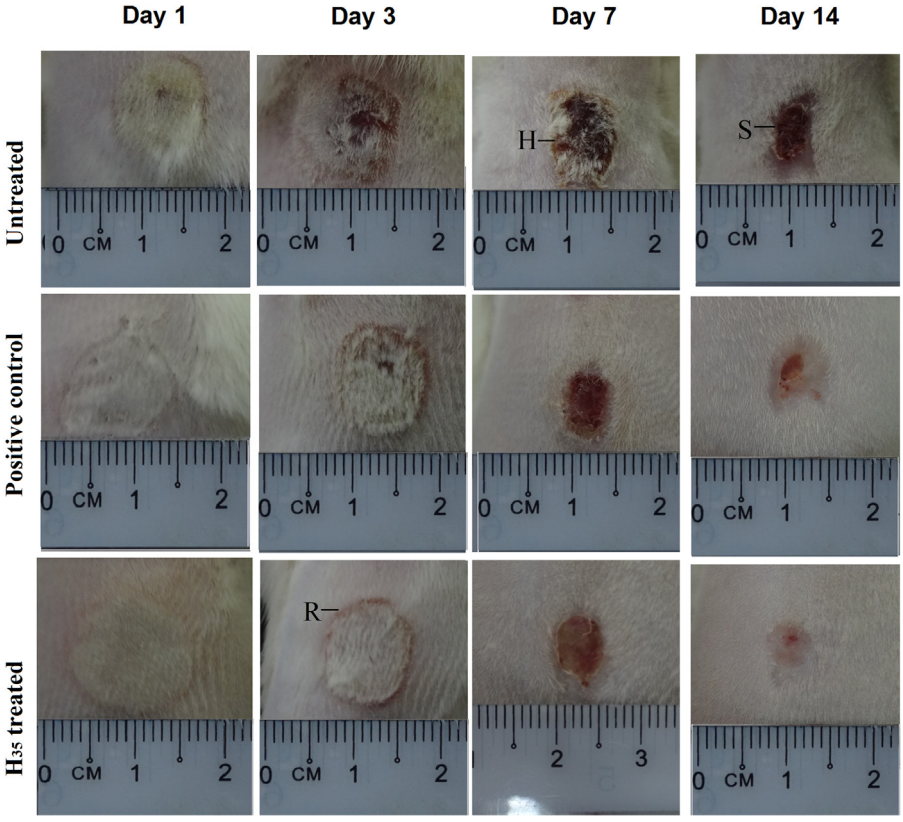

Fig. 4. Photographs on days 1, 3, 7, and 14 of wounds treated with H_{35}, the positive control treatment, or not treated. H, hemorrhage; R, redness; S, scab.

showed hemorrhagic, scabbed wounds. However, no scabbing was observed at the burn sites in the H_{35}-treated group. Differences in wound closure between the H_{35}-treated and control groups were determined by the sizes of scar grooves. The wounds treated with H_{35} and the positive control (Intrasite Comformable®) showed nearly complete healing as the treatment approached day 14, which was not observed in the untreated group. The wounds were considered to be completely healed once visible scabs were shed and a new epidermal layer had formed (Obara et al., 2003).

The rate of wound closure was evaluated by calculation of the open wound area as a function of time, as shown in Fig. 5. On day 1, there were no significant differences between the groups. However, on days 3, 7, and 14, H_{35}-treated burns showed a greater percentage of wound closure compared with the untreated burns. By day

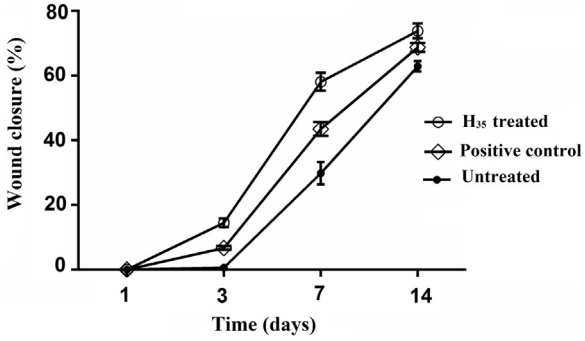

Fig. 5. Rate of wound healing of wounds treated with H_{35}, the positive control treatment, or not treated on days 1, 3, 7, and 14.

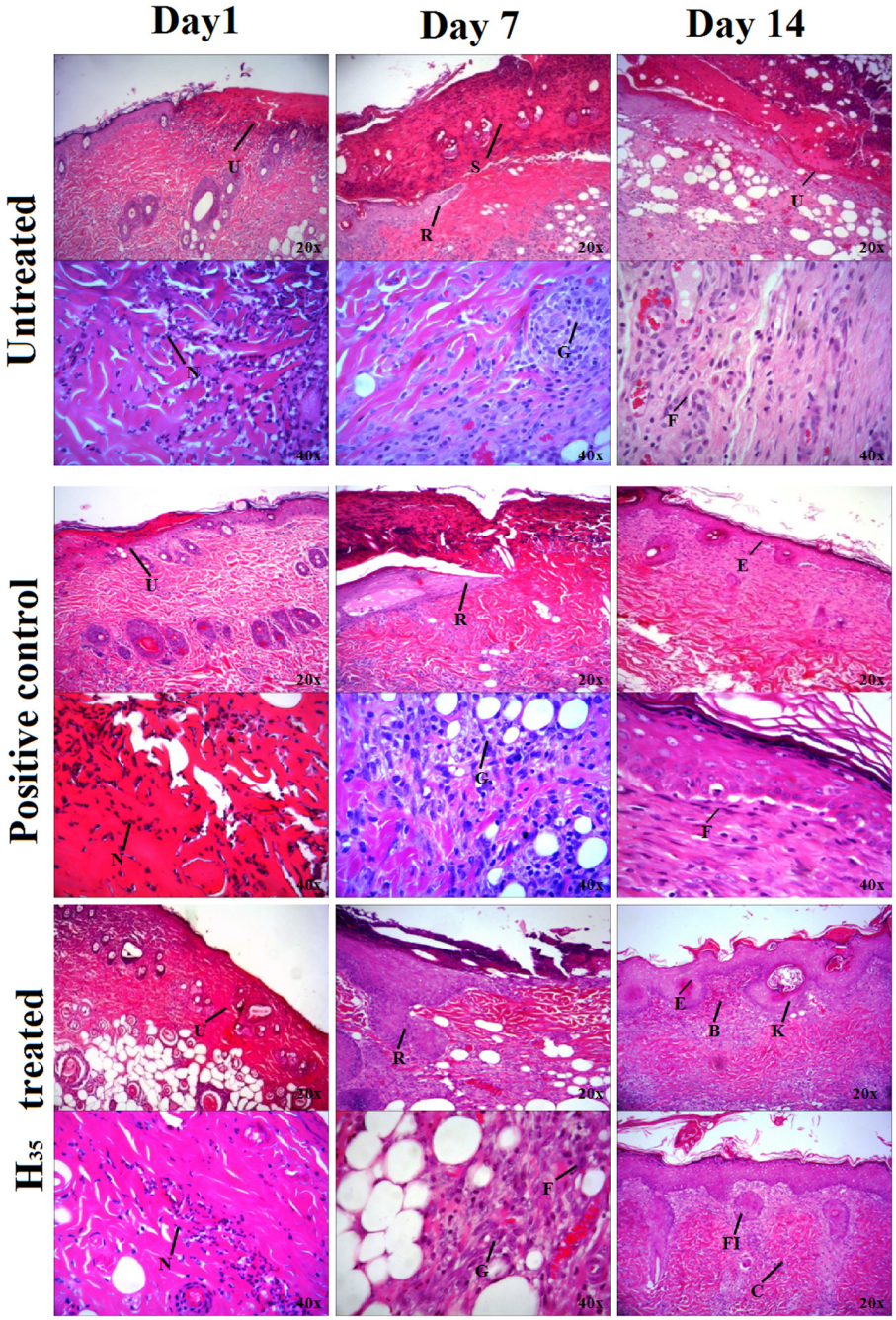

Fig. 6. Histopathological observations of the wound healing of various groups on days 1, 7, and 14 with H&E staining. Lines indicate wound healing events. B, blood vessels; C, collagen; E, epidermis; F, fibroblast cells; Fl, hair follicle; G, granulation tissue; K, keratin; N, neutrophils; R, reepithelialization; S, Scab; and U, ulceration. All the figures have been shown with the magnification at 20× and 40×.

7, 60% wound closure was observed in the H_{35}-treated group. In contrast, only 40% and 30% wound closure was observed on day 7 for the positive control and untreated groups. These results showed that the rate of wound healing with H_{35} hydrogel was higher than the positive control treatment or no treatment. This result was supported by macroscopic observations, in which showed that crusts formed and were shed much earlier in the H_{35} group than in the untreated group.

3.3.3. Histological observations

The healing patterns partial-thickness burns were studied by histological examination of the test and control samples at days 1, 7, and 14 post-burn by H&E staining (Fig. 6) and Masson's trichrome staining (Fig. 7). Microscopic observations on day 1 showed little difference between the groups. The epidermis showed an area of ulceration was covered with acute inflammatory cells, such as neutrophils. A thick layer of necrotic tissue was observed where neutrophils and other inflammatory cells were present. It has been shown that neutrophils most densely infiltrate wound areas, and appear along with smaller numbers of lymphocytes and macrophages (Fu et al., 2012). The primary function of neutrophils is to dispose of pathogens entrapped in the clot at the time of injury. Masson's trichrome staining revealed the epidermis was destroyed and the degradation of damaged collagen fibers was observed at the burn site.

At day 7, the epidermis in all groups showed extensive areas of ulceration and was covered by acute inflammatory exudates. For untreated and positive control groups, scab formation was observed on the epidermis. The underlying dermis and subcutaneous tissue showed necrosis and replacement by granulation tissue. In addition, regeneration of new epithelium had occurred in the untreated and positive control groups. In the H_{35} hydrogel-treated group, the scabs fell off earlier than in the other groups, and the underlying dermis and subcutaneous tissue were infiltrated by granulation tissue, neutrophils, newly formed blood vessels, and abundant fibroblasts. Active fibroblasts, responsible for the synthesis of collagen (Fig. 7), were clearly observed in the H_{35}-treated group. Epithelialization (marked thickening of new epidermis) at the wound site was increased in the H_{35}-treated group compared to the other groups. According to Lin et al. (2013), during the period from day 3 to day 10 of treatment, new epidermis rapidly grew from the margins of the wound sites to the centers.

By day 14, the untreated group showed the lowest re-epithelialization rate among the groups. The epidermis showed ulceration areas covered by acute inflammatory exudates. Infiltration of neutrophils and loss of skin adnexa were observed at the burn sites. Active fibroblasts showed signs of rapid growth. Burns treated with the positive control showed increased epithelialization and condensed nuclei of inactive fibroblasts. The number of fibroblasts gradually declines as the fibrous composition increases (Chen et al., 2013).

In comparison to the positive control, treatment with H_{35} markedly increased the formation of keratin and hair follicles, and the proliferation of blood vessels. The H_{35} and the positive control treatment groups showed organized superficial epithelium and were nearly healed.

Increased deposition of collagen was observed in all groups. However, collagen deposition in the dermis was more organized and compact in the H_{35} group compared to the positive control group and the untreated groups. The appearance of collagen was clearly observed in the H_{35} treatment group on day 14 (Fig. 7). This was likely a result of increased fibroblast proliferation on day 7 (Fig. 6), which promoted collagen deposition.

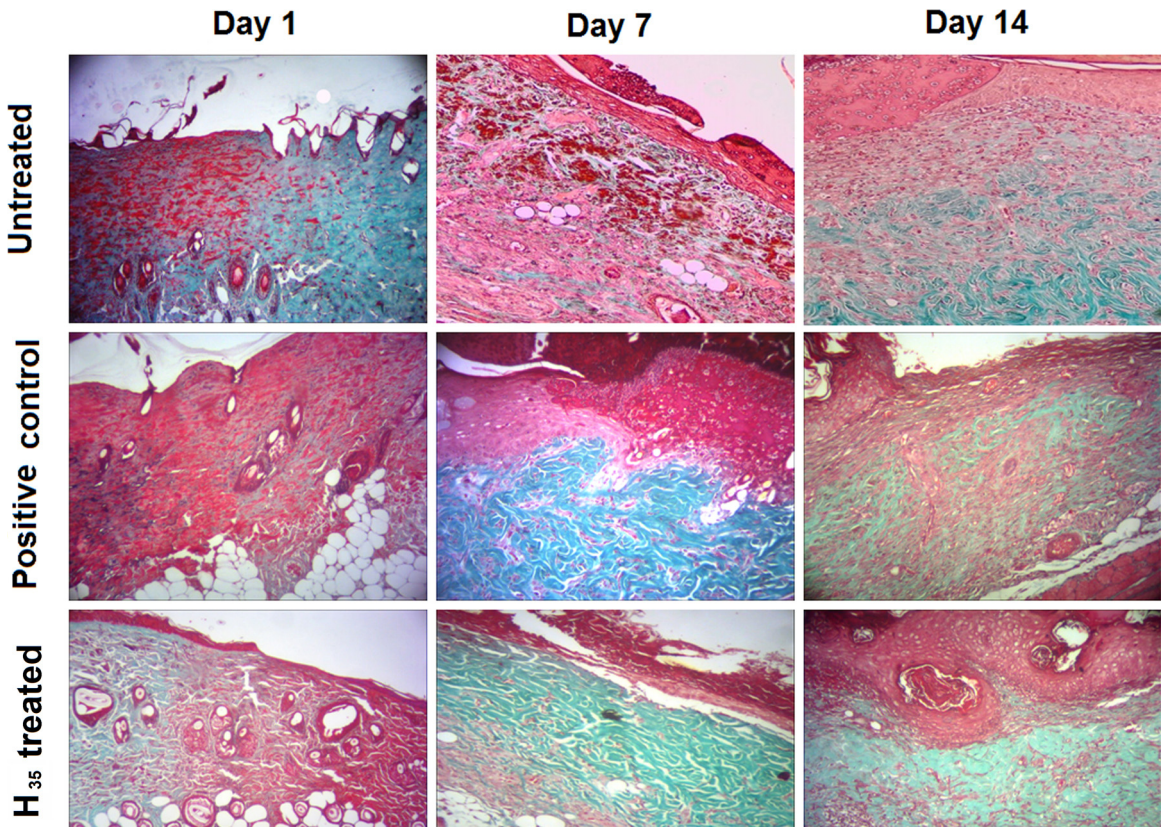

Fig. 7. Histopathological characteristics of wound healing in different treatment groups on days 1, 7, and 14 as observed with Masson's trichrome staining at 40× magnification.

4. Conclusions

In the present study, H_{35} and H_{50} hydrogels were prepared as wound dressings. H_{35} showed physical and mechanical characteristics that were more suitable for this purpose. A larger number of pores and a greater ability to swell helped the H_{35} hydrogel retain more water than the H_{50} preparation. H_{35} films were biocompatible with mouse fibroblasts for up to 48 h, and animal studies revealed that H_{35} accelerated healing by promoting neovascularization, re-epithelialization, and proliferation of fibroblasts. Thus, BC hydrogels with BC:AA at a 60:40 ratio synthesized with 35 kGy have the potential to be used for burn dressings.

Acknowledgements

The authors would like to thank Universiti Kebangsaan Malaysia (UKM) and Dr. Madhavan Manoharan for financial assistance and support. This project was funded by UKM (INOVASI-2013-005).

Appendix A. Supplementary data

Supplementary data associated with this article can be found, in the online version, at http://dx.doi.org/10.1016/j.carbpol.2014.08.025.

References

Ajji, Z., Mirjalili, G., Alkhatab, A., & Dada, H. (2008). Use of electron beam for the production of hydrogel dressings. *Radiation Physics and Chemistry*, *77*, 200–202.
Alsarra, I. A. (2009). Chitosan topical gel formulation in the management of burn wounds. *International Journal of Biological Macromolecules*, *45*, 16–21.
Amin, M. C. I. M., Abadi, A. G., & Katas, H. (2014). Purification, characterization and comparative studies of spray-dried bacterial cellulose microparticles. *Carbohydrate Polymers*, *99*, 180–189.
Amin, M. C. I. M., Ahmad, N., Halib, N., & Ahmad, I. (2012). Synthesis and characterization of thermo- and pH-responsive bacterial cellulose/acrylic acid hydrogels for drug delivery. *Carbohydrate Polymers*, *88*, 465–473.
Boateng, J. S., Matthews, K. H., Stevens, H. N. E., & Eccleston, G. M. (2008). Wound healing dressings and drug delivery systems: A review. *Journal of Pharmaceutical Sciences*, *97*, 2892–2923.
Chen, S., Tsao, C., Chang, C., Lai, Y., Wu, M., Chuang, C., et al. (2013). Assessment of reinforced poly(ethylene glycol) chitosan hydrogels as dressings in a mouse skin wound defect model. *Materials Science & Engineering. C, Materials for Biological Applications*, *33*, 2584–2594.
Czaja, W., Krystynowicz, A., Bielecki, S., & Brown, R. M., Jr. (2006). Microbial cellulose – The natural power to heal wounds. *Biomaterials*, *27*, 145–151.
Fu, L., Zhang, Y., Li, C., Wu, Z., Zhuo, Q., Huang, X., et al. (2012). Skin tissue repair materials from bacterial cellulose by a multilayer fermentation method. *Journal of Materials Chemistry*, *22*, 12349–12357.
Fu, L., Zhang, J., & Yang, G. (2013). Present status and applications of bacterial cellulose-based materials for skin tissue repair. *Carbohydrate Polymers*, *92*, 1432–1442.
Gupta, B., Plummer, C., Bisson, I., Frey, P., & Hilborn, J. (2002). Plasma-induced graft polymerization of acrylic acid onto poly(ethylene terephthalate) films: Characterization and human smooth muscle cell growth on grafted films. *Biomaterials*, *23*, 863–871.
Halib, N., Amin, M. C. I. M., & Ahmad, I. (2010). Unique stimuli responsive characteristics of electron beam synthesized bacterial cellulose/acrylic acid composite. *Journal of Applied Polymer Science*, *116*, 2920–2929.
Han, W., Tu, M., Zeng, R., Zhao, J., & Zhou, C. (2012). Preparation, characterization and cytocompatibility of polyurethane/cellulose based liquid crystal composite membranes. *Carbohydrate Polymers*, *90*, 1353–1361.
Huang, S., & Fu, X. (2010). Naturally derived materials-based cell and drug delivery systems in skin regeneration. *Journal of Controlled Release*, *142*, 149–159.
Ito, T., Yoshida, C., & Murakami, Y. (2013). Design of novel sheet-shaped chitosan hydrogel for wound healing: A hybrid biomaterial consisting of both PEG-grafted chitosan and crosslinkable polymeric micelles acting as drug containers. *Materials Science & Engineering C*, *33*, 3697–3703.
Khan, T. A., Peh, K. K., & Ch'ng, H. S. (2000). Mechanical, bioadhesive strength and biological evaluations of chitosan films for wound dressing. *Journal of Pharmacy & Pharmaceutical Sciences*, *3*, 303–311.
Kim, D., & Park, K. (2004). Swelling and mechanical properties of superporous hydrogels of poly(acrylamide-co-acrylic acid)/polyethylenimine interpenetrating polymer networks. *Polymer*, *45*, 189–196.
Kim, I. Y., Yoo, M. K., Seo, J. H., Park, S. S., Na, H. S., Lee, H. C., et al. (2007). Evaluation of semi-interpenetrating polymer networks composed of chitosan and poloxamer for wound dressing application. *International Journal of Pharmaceutics*, *341*, 35–43.
Kumar, P. T. S., Abhilash, S., Manzoor, K., Nair, S. V., Tamura, H., & Jayakumar, R. (2010). Preparation and characterization of novel β-chitin/nanosilver composite scaffolds for wound dressing applications. *Carbohydrate Polymers*, *80*, 761–767.
Lee, Y., Chang, J., Yang, M., Chien, C., & Lai, W. (2012). Acceleration of wound healing in diabetic rats by layered hydrogel dressing. *Carbohydrate Polymers*, *88*, 809–819.
Lin, W., Lien, C., Yeh, H., Yu, C., & Hsu, S. (2013). Bacterial cellulose and bacterial cellulose-chitosan membranes for wound dressing applications. *Carbohydrate Polymers*, *94*, 603–611.
Loo, Y., Wong, Y., Cai, E. Z., Ang, C., Raju, A., Lakshmanan, A., et al. (2014). Ultrashort peptide nanofibrous hydrogels for the acceleration of healing of burn wounds. *Biomaterials*, *35*, 1–10.
Mogoşanu, G. D., & Grumezescu, A. M. (2014). Natural and synthetic polymers for wounds and burns dressing. *International Journal of Pharmaceutics*, *463*, 127–136.
Obara, K., Ishihara, M., Ishizuka, T., Fujita, M., Ozeki, Y., Maehara, T., et al. (2003). Photocrosslinkable chitosan hydrogel containing fibroblast growth factor-2 stimulates wound healing in healing-impaired db/db mice. *Biomaterials*, *24*, 3437–3444.
O'Brien, J., Wilson, I., Orton, T., & Pognan, F. (2000). Investigation of the Alamar Blue (resazurin) fluorescent dye for the assessment of mammalian cell cytotoxicity. *European Journal of Biochemistry*, *267*, 5421–5426.
Peppas, N. A., Bures, P., Leobandung, W., & Ichikawa, H. (2000). Hydrogels in pharmaceutical formulations. *European Journal of Pharmaceutics and Biopharmaceutics*, *50*, 27–46.
Pham, C., Greenwood, J., Cleland, H., Woodruff, P., & Maddern, G. (2007). Bioengineered skin substitutes for the management of burns: A systematic review. *Burns*, *33*, 946–957.
Rhim, J. (2004). Physical and mechanical properties of water resistant sodium alginate films. *LWT – Food Science and Technology*, *37*, 323–330.
Said, H. M., Alla, S. G. A., & El-Naggar, A. W. M. (2004). Synthesis and characterization of novel gels based on carboxymethyl cellulose/acrylic acid prepared by electron beam irradiation. *Reactive and Functional Polymers*, *61*, 397–404.
Shah, N., Ul-Islam, M., Khattak, W. A., & Park, J. K. (2013). Overview of bacterial cellulose composites: A multipurpose advanced material. *Carbohydrate Polymers*, *98*, 1585–1598.
Soler, D. M., Rodríguez, Y., Correa, H., Moreno, A., & Carrizales, L. (2012). Pilot scale-up and shelf stability of hydrogel wound dressings obtained by gamma radiation. *Radiation Physics and Chemistry*, *81*, 1249–1253.
Wang, T., Zhu, X., Xue, X., & Wu, D. (2012). Hydrogel sheets of chitosan, honey and gelatin as burn wound dressings. *Carbohydrate Polymers*, *88*, 75–83.
Williams, D. F. (1999). *The Williams dictionary of biomaterials*. Liverpool: Liverpool University Press.
Yang, X., Zhu, Z., Liu, Q., Chen, X., & Ma, M. (2008). Effects of PVA, agar contents, and irradiation doses on properties of PVA/ws-chitosan/glycerol hydrogels made by γ-irradiation followed by freeze-thawing. *Radiation Physics and Chemistry*, *77*, 954–960.
Yu, C., Wu, Y., Zeng, F., Li, X., Shi, J., & Wu, S. (2013). Hyperbranched polyester-based fluorescent probe for histone deacetylase via aggregation-induced emission. *Biomacromolecules*, *14*, 4507–4514.
Zaborowska, M., Bodin, A., Bäckdahl, H., Popp, J., Goldstein, A., & Gatenholm, P. (2010). Microporous bacterial cellulose as a potential scaffold for bone regeneration. *Acta Biomaterialia*, *6*, 2540–2547.